catalysts

MDPI

Article

Copper-on-Magnetically Activated Carbon-Catalyzed Azide-Alkyne Click Cycloaddition in Water

Noura Aflak [1,*], El Mountassir El Mouchtari [1], Hicham Ben El Ayouchia [1,*], Hafid Anane [1], Salah Rafqah [1], Miguel Julve [2] and Salah-Eddine Stiriba [2,*]

[1] Laboratoire de Chimie Analytique et Moléculaire/LCAM, Faculté Polydisciplinaire de Safi, Université Cadi Ayyad, Safi 46030, Morocco
[2] Instituto de Ciencia Molecular/ICMol, Universidad de Valencia, C/Catedrático José Beltrán 2, 46980 Valencia, Spain
* Correspondence: noura.aflak@gmail.com (N.A.); belayou@gmail.com (H.B.E.A.); stiriba@uv.es (S.-E.S.)

Abstract: The copper-catalyzed cycloaddition of alkynes and azides (CuAAC) to give the corresponding 1,4-disubstituted-1,2,3-triazoles is the most successful and leading reaction within the click chemistry regime. Its heterogenization stands out as the innovative strategy to solve its environmental concerns and toxicity issue. In this report, magnetically retrievable activated carbon produced from biomass Persea Americana Nuts was loaded with a catalytically active copper(I) catalyst, resulting into a heterogeneous nanocatalyst, namely Cu-Fe_3O_4-PAC. This new compound was fully characterized using several techniques such as Powder X-ray diffraction (PXRD), Fourier-transform infrared spectroscopy (FT-IR), Scanning Electron Microscopy (SEM), Energy Dispersive X-ray diffraction (EDX), Brunauer–Emmett–Teller (BET) analysis, and Raman spectroscopy. Cu-Fe_3O_4-PAC catalyzed the cycloaddition of a variety of substituted terminal alkynes and organic azides in water at room temperature with excellent yields and in a regioselective manner. The hot filtration test demonstrated that no significant leaching of catalytically active copper particles took place during the CuAAC process, a feature that supports the stability of Cu-Fe_3O_4-PAC and its heterogeneous action way. Cu-Fe_3O_4-PAC was magnetically separable by applying an external magnetic field and was recyclable up to five runs, with only an 8% decline in its activity after the 5th catalytic test. The hot filtration experiment heavily suggested that the present catalytic system would proceed in a heterogeneous manner in CuAAC. The electronic characteristics, nature of the intermediate complexes, and type of ligand-to-copper bonding interactions were studied by using quantum theory of atoms in molecules (QTAIM) and natural bond orbital (NBO) calculations, which enabled the confirmation of the proposed binuclear mechanism.

Keywords: magnetic nanoparticles; activated carbon; copper; heterogeneous catalysis; CuAAC; QTAIM; NBO analysis

Citation: Aflak, N.; El Mouchtari, E.M.; Ben El Ayouchia, H.; Anane, H.; Rafqah, S.; Julve, M.; Stiriba, S.-E. Copper-on-Magnetically Activated Carbon-Catalyzed Azide-Alkyne Click Cycloaddition in Water. *Catalysts* **2022**, *12*, 1244. https://doi.org/10.3390/catal12101244

Academic Editor: Anna Maria Raspolli Galletti

Received: 14 September 2022
Accepted: 13 October 2022
Published: 15 October 2022

1. Introduction

The copper-catalyzed [3+2] cycloaddition of azides and alkynes (CuAAC) is the most popular and leading click chemistry concept [1], and has been successfully applied for the synthesis of 1,2,3-triazoles and is widely used in drug discovery, pharmaceutical and agrochemical technology [2–6] as well as in biology and material sciences [7–11]. CuAAC has the power to afford 1,4-disubstituted-1,2,3-triazole derivatives in a fast and regioselective manner under mild reaction conditions [12–14]. The in situ generated copper(I), either from copper(II) salt precursors, such as $CuSO_4 \cdot 5H_2O$, in the presence of a reducing agent, such as sodium ascorbate, or from a mixture of copper(0) and copper(II) species usually in the presence of a stabilizing ligand and/or a base, is the catalytically active agent that mediates the azide-alkyne ligation process [15]. The use of the copper catalyst, in particular, in the click of the 1,2,3-triazole derivatives with biological attributes has been largely questioned

due to environmental concerns and toxicity issues raised from the contents of copper species in such biological compounds [16]. This has led to the development of heterogeneous catalytic systems, which have allowed for efficient copper removal often through filtration or decantation methods. Most of the heterogeneous approaches of CuAAC click chemistry consists of immobilizing the copper species by employing microporous organic or inorganic solids [17–23]. In this context, activated carbon was found to be an efficient support in heterogeneous CuAAC click chemistry due to many chemical-specific features, including its inexpensive cost, availability, large surface area, porous structure, ample surface functional groups, and facile scalable synthesis [21–24]. However, the impractical work-up procedures such as filtration and centrifugation–decantation, which are required for the final separation of the source of heterogeneous copper(I) from the reaction medium, lead to the waste of the catalyst and/or reagents for their subsequent use. To overcome this problematic experimental issue and open the way to heterogeneous CuAAC click chemistry as a practical industrial chemical process, recent strategies have focused on the use of magnetically separable catalysts by using ferric oxide magnetic nanoparticles, such as Fe_2O_3, Fe_2O_4, and Fe_3O_4. They are easily separable by using an external magnetic field and are further recyclable in subsequent catalytic runs [25–27] (Figure 1).

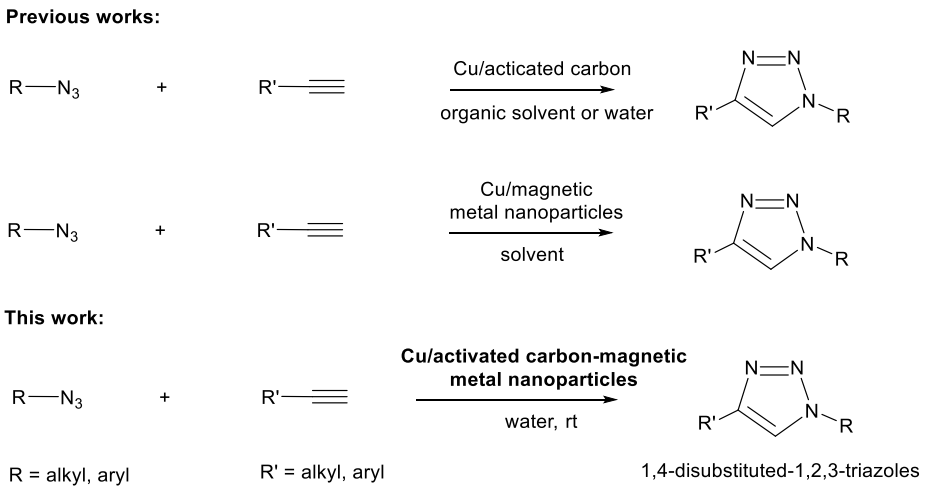

Figure 1. Click CuAAC performed under heterogeneous catalysis.

In the context of our main efforts to develop and add value to the benign heterogenization of CuAAC click chemistry [24], herein we report an ecofriendly heterogenization approach to the click of triazoles. It consists of the combination of activated carbon made up from agricultural wastes biomass such as *Persea Americana Nuts* with magnetic metal nanoparticles, followed by its loading with copper(I). This newly characterized source of heterogeneous copper(I) catalysts, namely (Cu-Fe_3O_4-PAC), exhibits an excellent catalytic performance in azide-alkyne cycloaddition processes in water at room temperature. The Cu-Fe_3O_4-PAC catalyst can be easily recovered by applying an external magnetic field and it can be recycled for additional runs without any loss of its selectivity.

2. Results and Discussion

2.1. Synthesis and Characterization of the Catalyst

The synthetic procedure used to prepare the Cu-Fe_3O_4-PAC catalyst is illustrated in Scheme 1. In the first step, the Powdered Activated Carbon (PAC) was prepared from the agricultural wastes biomass *Persea Americana Nuts* via the chemical activation method using orthophosphoric acid as the activating agent. In the second step, the prepared activated carbon was partially covered by Fe_3O_4 magnetic nanoparticles using the co-precipitation method of ferric ions (Fe^{2+}/Fe^{3+}) on the surface of the carbon. Finally, the magnetic carbon was impregnated with a copper(I) chloride solution to afford the final Cu-Fe_3O_4-PAC as a magnetic nanocomposite.

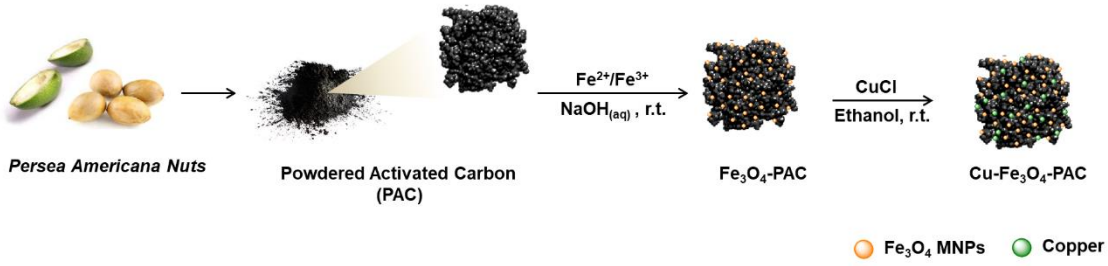

Scheme 1. Stepwise synthesis of Cu-Fe_3O_4-PAC.

The composition of the synthesized material was firstly analyzed with Powder X-ray diffraction (PXRD). As depicted in Figure 2, the obtained PXRD patterns displayed the following diffractions peaks (2θ [°]): 30.5, 35.9, 43.6, 53.9, 57.6, and 62.7. They were identified as the (220), (311), (400), (422), (511), and (440) crystalline planes of the cubic structure of Fe_3O_4 (JCPDS: 19-629) (Figure 2b,c) [28]. In addition, the presence of a low-intensity peak at 28.2° corresponded to the (111) crystalline plane of CuCl (JCPDS: 01-081-1841), which could be the predominance of the amorphous carbon in Cu-Fe_3O_4-PAC (Figure 2c) [29]. The presence of two peaks around 26 and 43° corresponding to the (002) and (100) crystalline planes were attributed to the microcrystalline graphitic structures present in amorphous carbon [30]. The decrease in or disappearance of the intensity peaks when these graphitic structures were covered with CuCl and/or Fe_3O_4 suggests that copper and/or iron oxide particles were formed on the carbon [30]. The same results were observed using Raman spectroscopy, as shown in Figure 3. The occurrence of two bands around 1320 and 1590 cm^{-1} indicated the presence of crystalline and amorphous carbon, respectively. The ratios between the D and G bands (I_D/I_G) confirmed the presence of a crystalline graphite part in amorphous carbon (Figure 3a) [31]. Furthermore, the decrease in the intensity of both the D and G bands in Fe_3O_4-PAC and Cu-Fe_3O_4-PAC confirmed that both Fe_3O_4 and Cu species were loading on the carbon surface (Figure 3b,c).

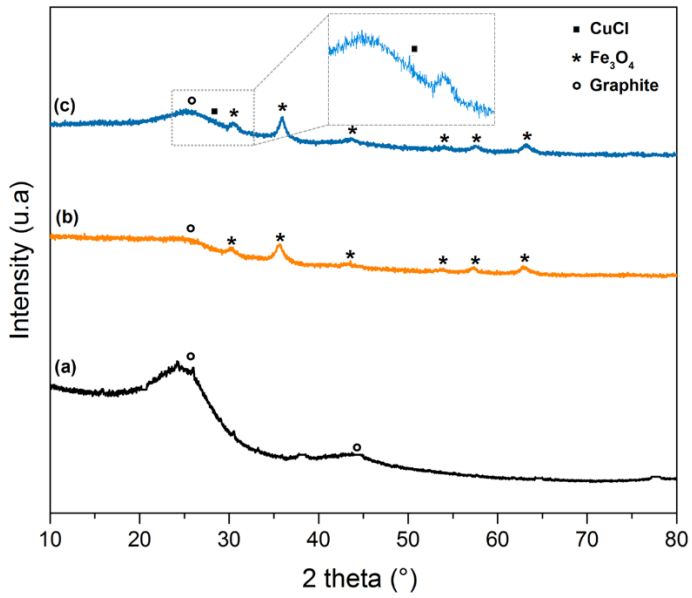

Figure 2. XRD spectra of PAC (**a**), Fe_3O_4-PAC (**b**), and Cu-Fe_3O_4-PAC (**c**).

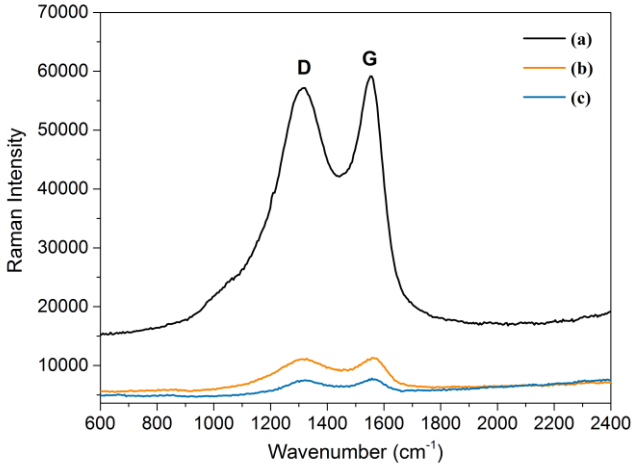

Figure 3. Raman spectra of PAC (**a**), Fe_3O_4-PAC (**b**), and Cu-Fe_3O_4-PAC (**c**).

The functional groups present in the PAC, Fe_3O_4-PAC, and Cu-Fe_3O_4-PAC samples are illustrated by their FT-IR spectra (Figure 4). The results showed the existence of absorption bands at 3409, 1558, 1391, 1158, and 1043 cm^{-1}, which correspond to the O−H, C=O, C=C, and C–O stretching vibrations from the surface of the carbon, respectively [32]. The occurrence of two broad bands at 631 and 561 cm^{-1} that are attributed to the stretching vibration of the Fe–O bonds confirm the formation of iron oxide (Fe_3O_4) [33]. The appearance of another weak absorption at 514 cm^{-1}, which are assigned to Cu–O bonds, suggests that copper is supported on the Fe_3O_4-PAC by the coordination of carbonyl groups (acetate or phosphate) with copper. In addition, the slight shift from 1558 cm^{-1} in Fe_3O_4-PAC to 1629 cm^{-1} in Cu-Fe_3O_4-PAC is mainly due to the coordination of the oxygen with the copper atom [34,35].

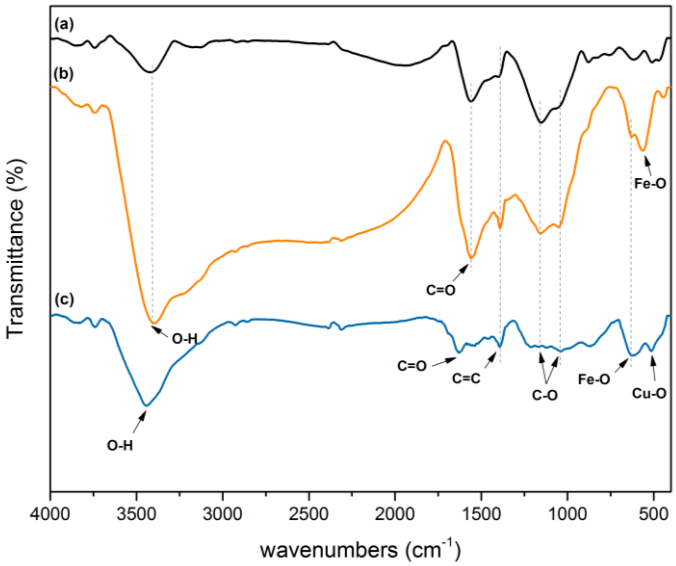

Figure 4. FT-IR spectra of PAC (**a**), Fe_3O_4-PAC (**b**), and Cu-Fe_3O_4-PAC (**c**).

The measurement of the porosity and surface area of the PAC, Fe_3O_4-PAC, and Cu-Fe_3O_4-PAC materials was carried out through the Brunauer–Emmett–Teller (BET) analysis as shown in Figure 5 and Table 1. The N_2 adsorption–desorption isotherm of all the carbon materials show a typical IV type pattern, according to the International Union of Pure and Applied Chemistry (IUPAC) classification, suggesting that these materials have mesoporous structures (Figure 5) [36]. Furthermore, the isotherms chang in a relatively

slight range of pressure, which further indicates that the pore structure of these materials is regular and the pore size distribution is uniform [37,38].

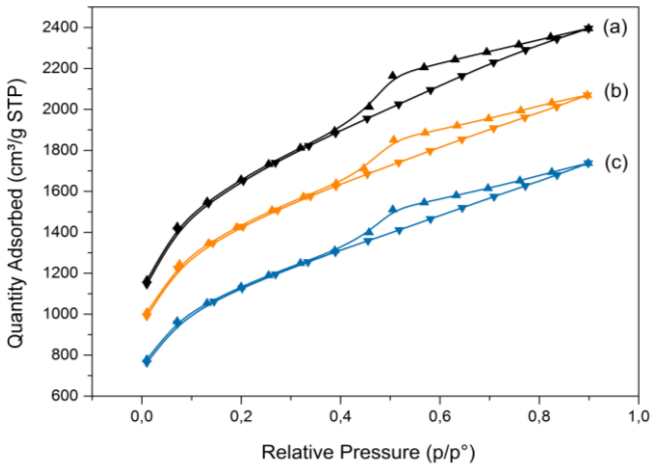

Figure 5. N_2 adsorption–desorption isotherm of PAC (**a**), Fe_3O_4-PAC (**b**), and Cu-Fe_3O_4-PAC (**c**).

With the N_2 adsorption–desorption measurements presented in Figure 5, the specific surface area and pore size distribution were calculated using the classic theory model of Barrett, Joyner, and Halenda (BJH) and the Brunauer–Emmett–Teller (BET) method, respectively (Table 1). As shown in Table 1, the results reveal that the pore diameters are within 2–50 nm, which further confirms that the materials are generally mesoporous. In addition, the specific surface area and total pore volume of the PAC materials decrease after impregnation with CuCl and/or Fe_3O_4 nanoparticles. This reduction could be explained by the fact that the copper and/or oxide iron nanoparticles occupy parts of the pores [39,40].

Table 1. Structural and textural characteristics of carbon materials calculated from dinitrogen sorption isotherms.

Material	Surface Area (m^2/g)	Pore Volume (cm^3/g)	Pore Size (nm)
PAC	5535.55	3.70	2.69
Fe_3O_4-PAC	4748.18	3.20	2.69
Cu-Fe_3O_4-PAC	3800.95	2.69	2.83

For further characterization, the surface morphology and chemical purity of the PAC, Fe_3O_4-PAC, and Cu-Fe_3O_4-PAC composites were determined using Scanning Electron Microscopy (SEM) and Energy-dispersive X-ray (EDX) analysis, respectively (Figures 6 and 7). The SEM images show general views of the composites, an irregular surface, and different size pores on the surface (Figure 6), features which agree with the BET analysis. The EDX analysis show the presence of carbon, oxygen, phosphorus, iron, chlorine, and copper (Figure 7). A weight percentage of copper of 1.01 wt% was determined with an Atomic Absorption Spectroscopy (AAS) analysis of the Cu-Fe_3O_4-PAC composites.

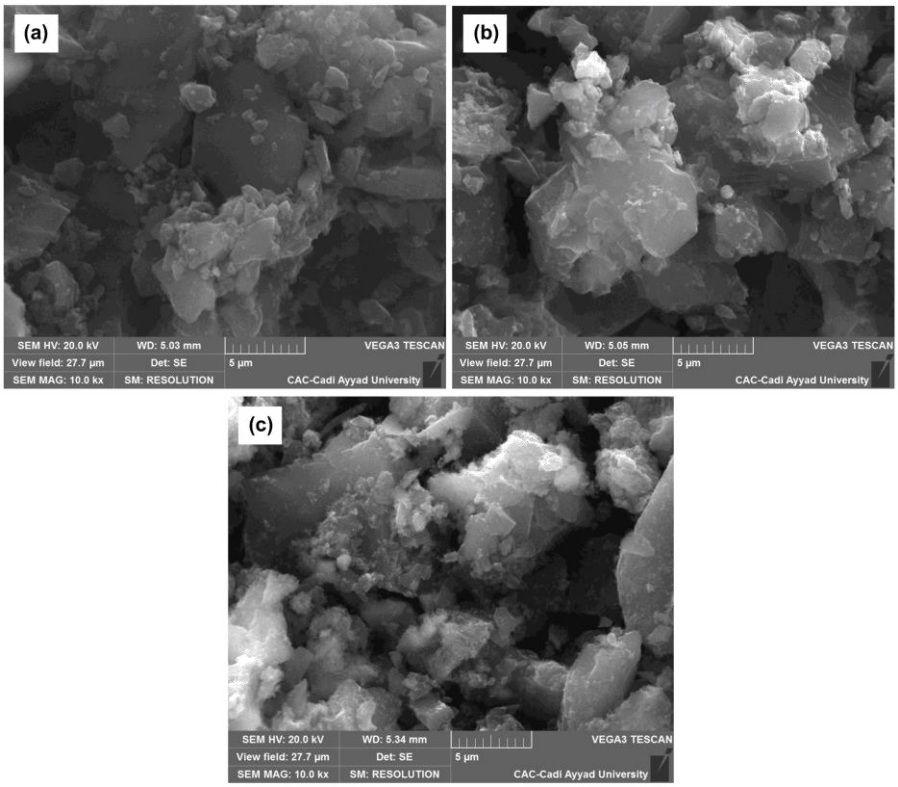

Figure 6. SEM images of PAC (**a**), Fe_3O_4-PAC (**b**), and Cu-Fe_3O_4-PAC (**c**).

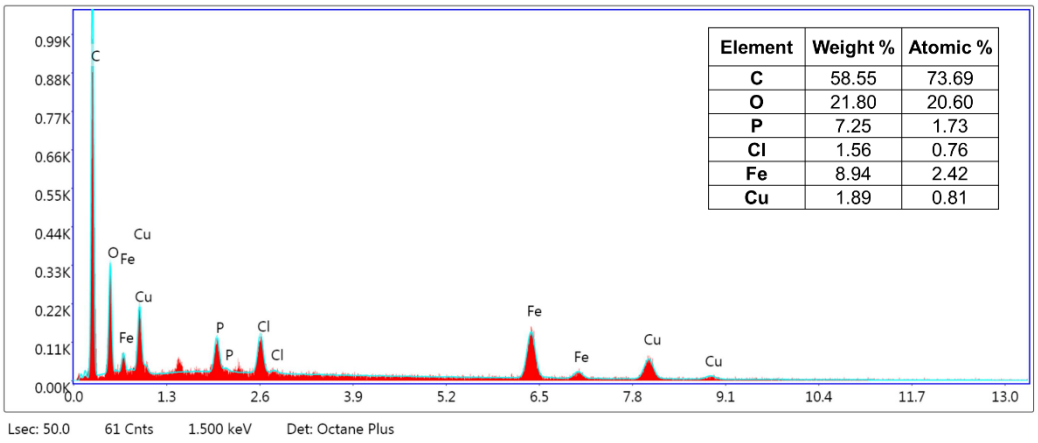

Element	Weight %	Atomic %
C	58.55	73.69
O	21.80	20.60
P	7.25	1.73
Cl	1.56	0.76
Fe	8.94	2.42
Cu	1.89	0.81

Figure 7. EDX spectrum of the Cu-Fe_3O_4-PAC catalyst.

2.2. Catalytic Studies

Once prepared and fully characterized, the catalytic activity of Cu-Fe_3O_4-PAC was tested in the click approach synthesis of 1,4-disubstituted-1,2,3-triazoles with copper-catalyzed azide-alkyne [3+2] cycloaddition reactions. Aiming at optimizing the synthesis of 1,4-disubstituted-1,2,3-triazoles under the click chemistry regime, the reaction between benzyl azide and phenylacetylene was selected as a model reaction. Initially, the reaction was carried out in the absence of a copper catalyst, and as expected, no product was formed (entry 1, Table 2). The same result was obtained when the PAC, Fe_3O_4, and Fe_3O_4-PAC were used (entries 2–4, Table 2). We next investigated the catalyst amount in the model catalytic cycloaddition reaction (entries 5–7, Table 2). As shown in Table 2, the decreasing of the Cu-Fe_3O_4-PAC amount to 50 mg did not modify the yield of the reaction (entries 5–6, Table 2). However, further decreasing of the Cu-Fe_3O_4-PAC amount to 30 mg caused a downturn in the yield to 64% (entry 7, Table 2). Thus, 50 mg of the Cu-Fe_3O_4-PAC catalyst

was found to be the optimum amount to catalyze the click synthesis of 1,4-disubstituted-1,2,3-triazole from the cycloaddition of benzyl azide and phenylacetylene. The solvent effect was also investigated (entries 8–14, Table 2). The results showed that the use of water and acetonitrile as solvents resulted in higher yields than those with other organic solvents, such as dichloromethane, THF, hexane, and EtOH (entries 6,8–12, Table 2). Furthermore, a good yield was also achieved by working in EtOH/H_2O and CH_3CN/H_2O as mixed solvents within the same reaction time (entries 13–14, Table 2). Therefore, we selected water as the ideal benign solvent to carry out the click synthesis of 1,4-disubstituted-1,2,3-triazoles under Cu-Fe_3O_4-PAC-catalyzed azide-alkyne [3+2] cycloaddition reactions. Consequently, 2.2 mol% of the Cu-Fe_3O_4-PAC catalyst in water as a solvent at room temperature were indeed the optimal reaction conditions for the synthesis of 1,4-disubstituted-1,2,3-triazoles.

Table 2. Optimization studies [a].

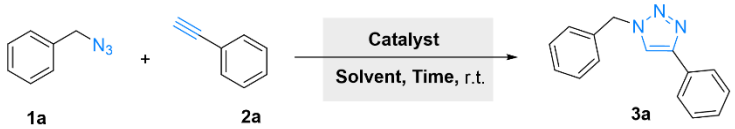

1a 2a 3a

Entry	Catalyst	Amount of Catalyst and Copper Loading (mg; mol%)	Solvent	Time (h)	Yield (%) [b]
1	-	-	H_2O	48	Trace
2	PAC [c]	30; 0	H_2O	48	Trace
3	Fe_3O_4 [c]	30; 0	H_2O	24	Trace
4	Fe_3O_4-PAC [c]	30; 0	H_2O	48	Trace
5	Cu-Fe_3O_4-PAC	70; 3.2	H_2O	22	99
6	Cu-Fe_3O_4-PAC	50; 2.2	H_2O	22	99
7	Cu-Fe_3O_4-PAC	30; 1.3	H_2O	22	64
8	Cu-Fe_3O_4-PAC	50; 2.2	EtOH	22	57
9	Cu-Fe_3O_4-PAC	50; 2.2	CH_3CN	27	98
10	Cu-Fe_3O_4-PAC	50; 2.2	Hexane	23	62
11	Cu-Fe_3O_4-PAC	50; 2.2	THF	46	55
12	Cu-Fe_3O_4-PAC	50; 2.2	Dichloromethane	24	30
13	Cu-Fe_3O_4-PAC	50; 2.2	EtOH/H_2O (1:1 *v*/*v*)	22	95
14	Cu-Fe_3O_4-PAC	50; 2.2	CH_3CN/H_2O (1:1 *v*/*v*)	22	93

[a] Reaction conditions: benzyl azide (0.376 mmol), phenylacetylene (0.352 mmol), solvent (5 mL), and catalyst were mixed and stirred at room temperature. [b] Isolated yield. [c] Reaction performed in the absence of copper salts.

After optimizing the conditions of the Cu-Fe_3O_4-PAC-catalyzed azide-alkyne [3+2] cycloaddition reaction, the scope and generality of this new protocol were investigated by using several organic azides and terminal alkyne derivatives to regioselectively afford 1,4-disubstituted-1,2,3-triazoles (Scheme 2). The results revealed that the reactions of terminal alkynes and organic azides with both electron-donating and electron-withdrawing substituents did not have any particular effect, with most of them being completed within 23 h as a maximum time and resulting in one regioisomer in high to excellent yields of the final 1,2,3-triazole products (Scheme 2). All the 1,4-disubstituted 1,2,3-triazole isomers were characterized by melting points and NMR spectroscopy. Some of them were purified by recrystallization from a mixture of dichloromethane/hexane when necessary (see Supplementary Materials).

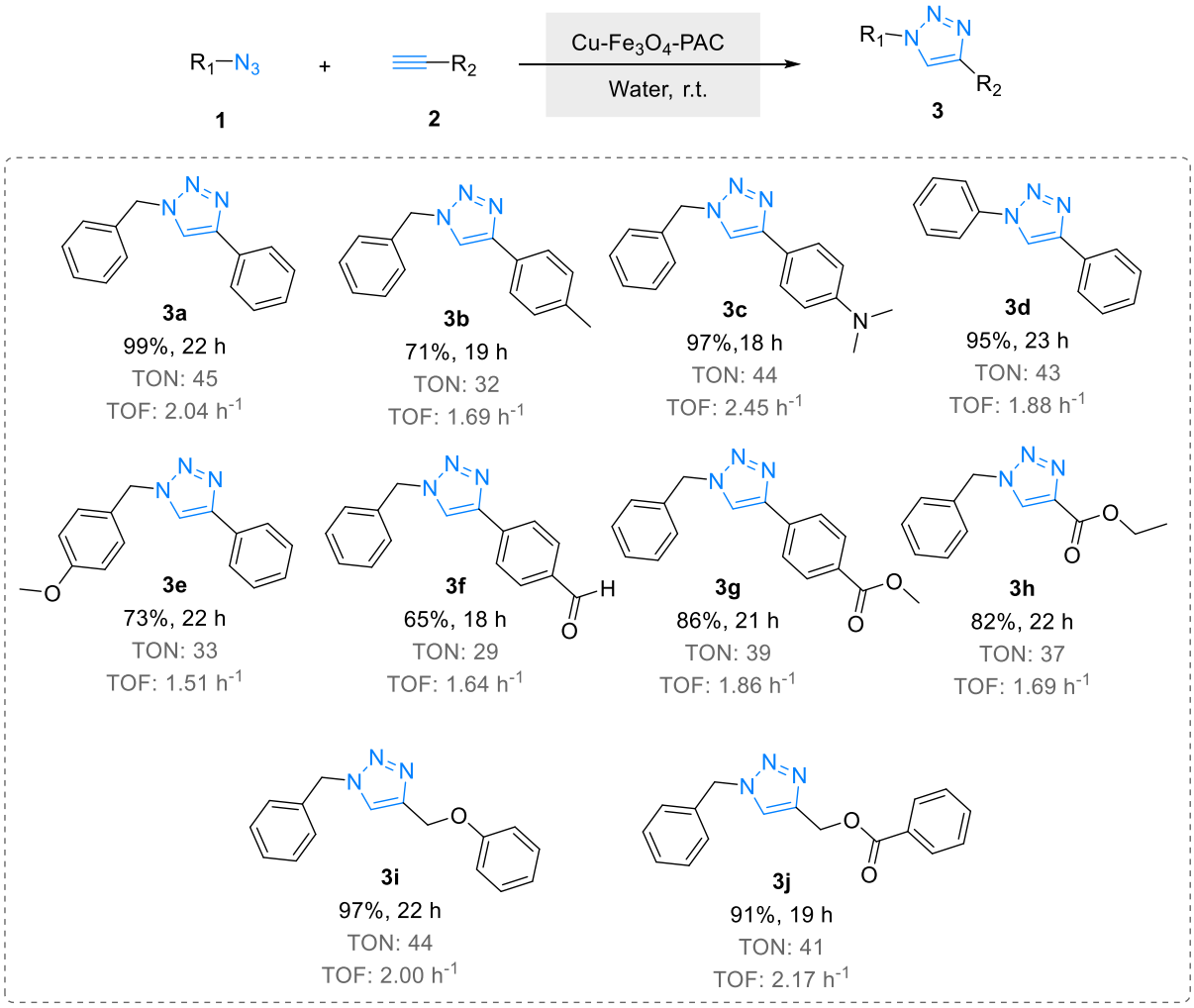

Scheme 2. Azide-alkyne [3+2] cycloaddition reactions catalyzed by Cu-Fe_3O_4-PAC. Abbreviations: TON = Turnover number (moles substrate/moles of catalyst), TOF = Turnover frequency (TON/time of reaction).

The recyclability of heterogeneous catalysts is an important issue from different points of view, such as environmental concerns and commercial applicability. To examine this issue, the recovery and reusability of Cu-Fe_3O_4-PAC were studied in the selected model reaction in the same conditions as the reactions. The catalyst was separated very easily by applying an external magnetic field, as shown in Figure 8, and then it was recovered and reused several times without adding further fresh catalyst.

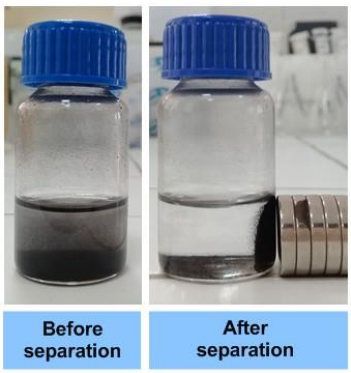

Figure 8. Magnetic separation of the Cu-Fe_3O_4-PAC catalyst with an external magnetic field.

After the completion of the reaction, the catalyst was separated from the reaction mixture, washed with dichloromethane and ethanol several times, dried in air overnight, and then reused in the next run. The results are presented in Figure 9, demonstrating that the catalyst was successfully reused for five cycles with only an 8% decline in its activity after the fifth test. This observation indicated the good stability and reusability of the Cu-Fe_3O_4-PAC catalyst. Furthermore, the percentage of copper particles in the final clickable triazole product was determined with an AAS analysis, and we found that they were present in a very low concentration (less than 0.3 ppm).

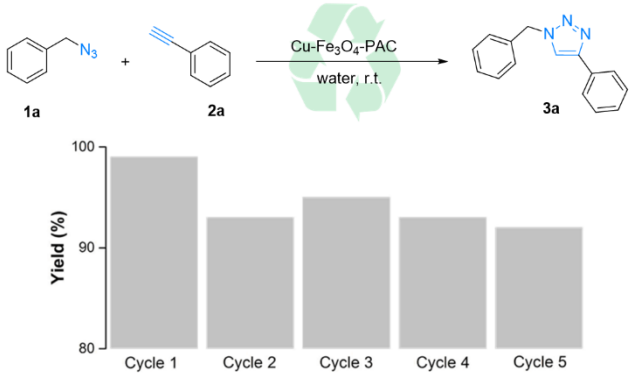

Figure 9. Yields of the Cu-Fe_3O_4-PAC catalyst in the cycloaddition of benzyl azide **(1a)** and phenylacetylene **(2a)** after five cycles of recovery/reuse.

To further confirm the stability of the catalyst under the heterogeneous phase, a hot filtration test was conducted (Figure 10). The reaction of benzyl azide **(1a)** and phenylacetylene **(2a)** was initiated at 50 °C in water under air atmosphere. After 2 h, the catalyst was recovered with an external magnet at the reaction temperature and the filtrate was allowed to react under the same catalytic reaction conditions. A slight conversion was observed after 10 h, indicating that the copper contents remained intact in the magnetically activated carbon, with slight leaching in the aqueous medium, as found by the click of the 1,2,3-triazole product.

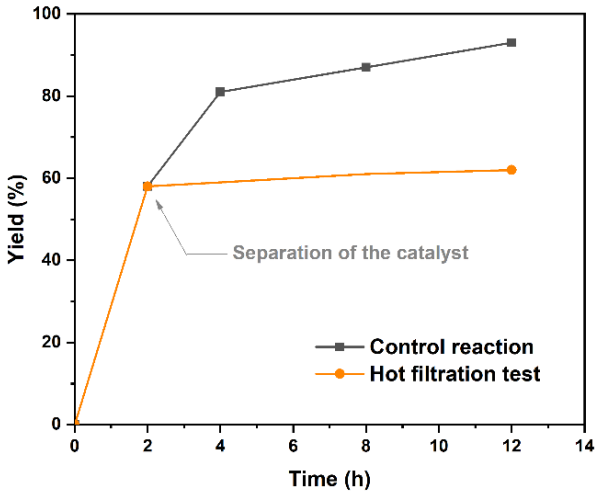

Figure 10. Hot filtration test in the azide-alkyne cycloaddition reaction catalyzed by Cu-Fe_3O_4-PAC.

2.3. Comparison of the Cu-Fe_3O_4-PAC Catalyst with Other Heterogeneous Catalysts

The comparison of the catalytic activity of the prepared CuCl-Fe_3O_4-PAC catalyst *versus* other heterogeneous catalysts in the click [3+2] cycloaddition reaction of benzyl azide **(1a)** and phenylacetylene **(2a)** is summarized in Table 3. Although CuAAC mediated by the CuCl-Fe_3O_4-PAC catalyst took longer compared with CuAAC mediated by other

heterogenous copper-based catalysts, with either carbon support or magnetic nanoparticles, in addition to having the lowest TON and TOF values, this new heterogeneous catalyst still has several advantages, including the occurrence in a quantitative yield, benign catalytic protocol, and easy separation from the liquid reaction phase via the application of an external magnetic field (Table 3).

Table 3. Comparison of the catalytic activity of the Cu-Fe_3O_4-PAC catalyst with other heterogeneous copper-based catalytic systems reported in the literature.

Entry	Catalyst [a] (Copper Loading)	Solvent/T (°C)	Base	Time	Yield (%)	TON/TOF	Ref.
1	Cu-Fe_3O_4-PAC (2.2 mol%)	H_2O/r.t.	-	22 h	99%	45/2.04 h^{-1}	This work
2	Cu-CANS (1 mol%)	H_2O/r.t.	-	6 h	98%	190/31.66 h^{-1}	[24]
3	Cu/C (10 mol%)	Dioxane/60 °C	Et_3N	10 min	99%	-	[21]
4	Cu_2O/C (5 mol%)	*i*-PrOH:H_2O/r.t.	Et_3N	2 h	82%	1957/13.5 h^{-1}	[41]
5	Cu@FeNP (5 mol%)	H_2O/r.t.	-	12 h	93%	-	[42]
6	CS-Fe_3O_4-Cu (1.54 mol%)	DCM/r.t.	-	12 h	92%	59.7/4.98 h^{-1}	[27]
7	$Cu(OH)_x/Al_2O_3$ (1.5 mol%)	Toluene/60 °C	-	30 min	95%	-	[43]

[a] Abbreviations: PAC = Powdered Activated Carbon; CANS = Carbon *Argan Nut Shells*; C = charcoal; CS = chitosan; r.t. = room temperature.

2.4. Mechanistic Insight

The most likely mechanistic CuAAC pathways for the formation of the regioselective 1,4-disubstituted-1,2,3-triazoles by using the Cu-Fe_3O_4-PAC as a catalyst is proposed based on our previous work [44] (Scheme 3) with a QTAIM and NBO analysis (see the Supplementary Materials). In this respect, the strength of the studied N_{azide}→Cu and C_{alkyne}→Cu interactions were investigated by means of the second-order stabilization energy $E^{(2)}$, given that a high value of this parameter indicates a greater intensity of the donor–acceptor interaction. The acceptor orbital, electron donor orbital, and the possible high interactions are listed in Table 4. In the first step, the catalytically active copper(I) species binds to the terminal alkyne to form the dinuclear copper-acetylide intermediate **(4)**, with the anti-bonding BD*(C−C) of the alkyne acting as a donor and the LP*(Cu) of the catalyst being an acceptor. The calculated value of this interaction was 4.34 kcal/mol. Then, the organic azide coordinates with the copper atom by means of the nitrogen atom, which is proximal to carbon atom, forming a reactive complex RC **(5)**, with the lone pair of azide (LP(N_{azide})) acting as a donor and the LP*(Cu) acting as an acceptor, with a stabilization energy $E^{(2)}$ of 12.95 kcal/mol. Afterwards, the distal nitrogen of the azide in RC can coordinate with the C-2 carbon of the acetylide, producing an intermediate of a six-membered copper-metalated triazolide **(6)**. The last step is a protonation of the copper triazolide **(7)** to afford the final 1,2,3-triazole product as 1,4-regioisomer **(8)**.

Table 4. NBO analysis for the intermediate complexes in the CuAAC reaction.

Complex	$E^{(2)}$ Energy (kcal/mol)	
	BD*(C_C)→LP*(Cu)	LP(N_{azide})→LP*(Cu)
4	4.34	-
5	5.86	12.95
6	2.69	30.72

A supporting view to that given by the NBO computations can be provided by the topology analysis of the electron density in the framework of the Quantum Theory of Atom in Molecules (QTAIM) suggested by Bader [45]. The topological analysis of the electron density distribution was carried out by means of Bader's theory, as implemented in the Multiwfn 3.3.9 software [46]. The topology analysis of the electron density was used to search the critical points. As can clearly be seen from molecular graphs of the studied

complexes (Figure 11), the BCPs and bonding lines were clearly found in addition to the ring BCPs.

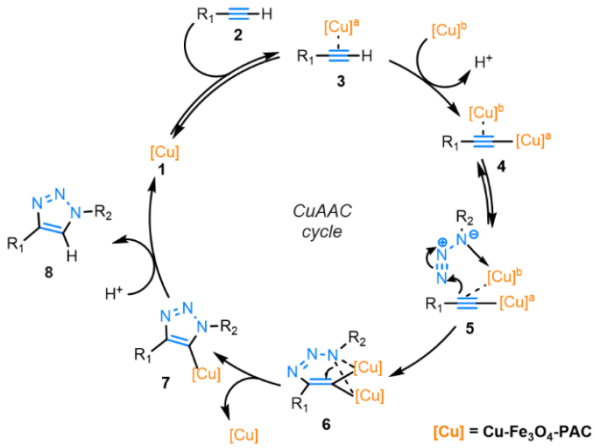

Scheme 3. Proposed mechanism of the Cu-Fe_3O_4-PAC-catalyzed azide-alkyne cycloaddition.

In order to figure out the nature of the ligand-to-copper interactions, Bader's QTAIM analysis [45] was used. Topological analyses of the electron density and its Laplacian were carried out at the bond critical points. The indicators of the copper–ligand bond that were applied were the electron densities $\rho(r)$, the Laplacians $\nabla^2\rho(r)$, the potential energy density $\nu(r)$, and the local kinetic electron energy density $G(r)$, which was computed at the bond critical points (BCPs) [47]. Depending on the sign of the $\nabla^2(r)$, the ligand-to-metal interactions were covalent (shared shell) or electrostatic (closed shell) if $\nabla^2\rho(r)$ was negative or positive, respectively. Furthermore, the $-G(r)/\nu(r)$ ratio was used for a further evaluation of the nature of the metal–ligand bonds. In this respect, the nature of the metal–ligand interaction was noncovalent or partly covalent if $-G(r)/\nu(r) > 1$ and $0.5 < -G(r)/\nu(r) < 1$, respectively. This ratio combined with the electron density ($\nabla^2(r)$) is applicable to determine the intermediate interactions and closed-shell interaction: ($-G(r)/\nu(r) < 1$ and $\nabla^2\rho(r) < 0$) and ($-G(r)/\nu(r) > 1$ and $\nabla^2\rho(r) < 0$), respectively.

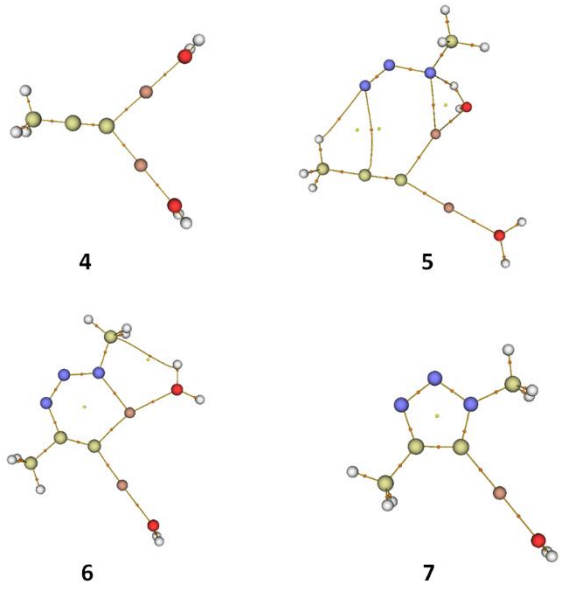

Figure 11. Molecular graphs of the computed intermediate complexes based on their gas phase optimized geometries at the M06-2X/6-311G(d,p), (LANL2DZ for Cu) level of theory. The BCPs are the small orange spheres around the center of the bond paths. The bond paths are the brown colored lines.

The calculated parameters at some BCPs in the studied complexes are summarized in Table 5. One can see therein that all $\nabla^2(r)$ values were negative, a feature that indicated that all of the interactions were shared shell for both the Cu—N_{azide} and Cu—C_{alkyne} interactions. Moreover, all the $\rho(r)$ values of the Cu—N and Cu—C bonds were in the range 0.11 to 0.98 au. This means that all of the interactions had some degree of an ionic, or rather polar ionic, character. In addition, the values of $-G(r)/\nu(r)$ for Cu—N_{azide} and Cu—C_{alkyne} were in the range 0.81–0.96, pointing out that these interactions were partly covalent. This conclusion was further supported by the medium (−40.78 kcal/mol) and high (−307.48 kcal/mol) values of the energy for the Cu—C_{alkyne} and Cu—N_{azide} interactions, respectively. The fact that the computed values of ELF were in the range 0.11–0.97 supports the occurrence of metallic bonding [48].

Table 5. Topological parameters of the copper–ligand interaction for the optimized structures of the intermediate complexes at M06-2X/6-311G(d,p) LANL2DZ for Cu.

Complex	Bonding Interaction	$\rho(r)$	$\nabla^2(\rho(r))$	$G(r)$	$\nu(r)$	$-G(r)/\nu(r)$	$\eta(r)$ [b]	E_{int} [a]
4	Cu—C_{alkyne}	0.98	−0.92	0.11	−0.13	0.84	0.22	−40.78
5	Cu—N_{azide}	0.66	−0.64	0.95	−0.98	0.96	0.97	−307.48
6	Cu—N_{azide}	0.87	−0.87	0.13	−0.14	0.92	0.11	−43.92
7	Cu—$C_{triazole}$	0.11	−0.11	0.13	−0.16	0.81	0.26	−50.20

[a] $E_{int} = 0.5\ \nu(r)$ (Kcal/mol); [b] the ELF $\eta(r)$ values are evaluated at the BCP.

3. Materials and Methods

3.1. Materials and Instrumental Facilities

Solvents and starting materials were used directly as purchased from commercial sources without further purification. The organic azide derivatives were synthesized according to the literature [24]. The reactions were carried out with continuous stirring under ambient conditions. Organic phases were dried using anhydrous $MgSO_4$ and were concentrated under reduced pressure. Thin-layer chromatography (TLC) was performed on commercial aluminum-backed plates of silica gel (Merck Kieselgel 60 F_{254}, Madrid, Spain) to determine the purity of the synthesized products. The visualization was performed under UV light at λ = 254 nm. The melting points of the final organic products were determined by means of an Electrothermal IA9100, France), employing the capillary tubes. ^{1}H NMR and ^{13}C NMR spectra were recorded on a spectrometer Brucker AC-300 MHz, Ettlingen, Germany (300 and 75 MHz for proton and carbon, respectively) in $CDCl_3$ as a solvent. The high-resolution mass spectra (HR-MS) were registered in the EI (70 eV) or FAB mode at the mass spectrometry service of the University of Valencia. The Scanning Electron Microscopy (SEM) and Energy-dispersive X-ray spectroscopy (EDX) analysis were performed on a VEGA3 TESCAN microscope and a high-resolution JEOL Field Emission Gun-Scanning Electron Microscope (FEG-SEM). Raman spectra were obtained by using a microscope confocal Raman spectrometer "SOL Instruments Confotec MR 520". FT-IR spectra were carried out on a FT-IR spectrophotometer (FT-IR Nicolet 5700). A Micromeritics 3-FLEX instrument (Haan, Germany) was used to examine the dinitrogen adsorption and desorption properties for all the samples. Specific surface areas were calculated with the Brunauer–Emmett–Teller (BET) method whereas the pore size distribution was estimated from the dinitrogen adsorption isotherms with the classic theory model of Barrett, Joyner, and Halenda (BJH). Atomic Absorption Spectroscopy (AAS) (Aurora AI800, Vancouver, Canada) was used to determine the copper contents in the synthesized materials.

3.2. Computational Details

All molecular geometries reported in this contribution were fully optimized by using the M06-2X functional with the 6-311G (d,p) basis set for the C, N, and H nuclei. Additionally, the LANL2DZ basis set was used for Cu and included in the GAUSSIAN 09 package [49]. A comprehensive analysis of the natural bond orbitals was performed for

all complexes and intermediates via NBO calculations in order to understand the various second-order interactions between the filled orbital of one subsystem and the empty one of another subsystem, which are measures of the intermolecular delocalization or hyperconjugation. The donor–acceptor interactions in the NBO basis were investigated by using the second-order Fock matrix [50]. For each donor (i) and acceptor (j), the stabilization energy E^2 associated with $i \rightarrow j$ delocalization for a donor NBO(i) and an acceptor NBO(j) was calculated using the following equation:

$$E^2 = q_{ij} \frac{F^2(i,j)}{\varepsilon_j - \varepsilon_i} \quad (1)$$

In this expression, q_{ij} represents the ith donor orbital occupancy, F_i and F_j are diagonal elements, and $F(i,j)$ stands for the off-diagonal elements linked to the NBO Fock matrix.

3.3. Preparation of the Powdered Activated Carbon (PAC)

The *Persea Americana Nuts* (PAN) were collected, cut, rinsed several times with double-distilled water to remove impurities, and then dried at room temperature for several days. The raw material was crushed to fine powder with a plunger ball mill. Then, it was mixed with phosphoric acid in a 1:1 H_3PO_4/PAN weight ratio by the plaster mill with a speed of 400 rpm/min for 10 min. The obtained mixture was then dehydrated at 120 °C for 4 h. After drying, the resulting material was carbonized in a muffle furnace at 500 °C for 1 h in an air atmosphere. The activated solid was crushed to a fine powder, and then it was washed several times with an aqueous solution of 0.1 M HCl, then with hot double-distilled water, and then finally with cold distilled water until neutralization (pH = 7). The washed material was dried completely, crushed, and kept in a hermetic glass bottle in a desiccator for further use.

3.4. Preparation of the Magnetically Powdered Activated Carbon (Fe_3O_4-PAC)

A total of 0.5 g of $FeCl_3 \cdot 6H_2O$ and 0.25 g of $FeCl_2 \cdot 4H_2O$ were dissolved in 40 mL of double-distilled water and stirred magnetically at room temperature. After stirring for about 10 min, an aqueous solution of 1 M NaOH was added dropwise to the stirring solution until pH = 10. Then, 2 g of PAC was dispersed into the mixture solution under ultrasonic stirring for 30 min and the solution was stirred for an additional 2 h at room temperature. The final product was recovered and washed several times using double-distilled water and was dried in the oven overnight at 180 °C.

3.5. Synthesis of the Cu-Fe_3O_4-PAC Catalyst

A total of 1 g of Fe_3O_4-PAC was added to a solution of copper(I) chloride (250 mg) in ethanol (40 mL), and the solution was stirred with a mechanical stirrer overnight at room temperature. The resulting material was recovered by using an external magnetic field, washed with ethanol as well as double-distilled water several times, and dried under a vacuum overnight.

3.6. General Procedure for the Synthesis of 1,2,3-triazole Derivatives

Azide (0.376 mmol, 1.07 equivalent), alkyne derivative (0.352 mmol, 1 equivalent), and Cu-Fe_3O_4-PAC (2.2 mol%) were placed in a reaction tube, and 5 mL of water were added. The mixture was stirred at room temperature and was monitored with TLC using ethyl acetate/hexane as an eluant. After the completion of the reaction, the reaction mixture was diluted by dichloromethane and the catalyst was separated by an external magnetic field, washed several times with dichloromethane and ethyl acetate, and dried under a vacuum. Then, organic solvents were evaporated under reduced pressure to give the corresponding 1,2,3-triazole derivative. The final product was further purified, when necessary, via recrystallization from dichloromethane/*n*-hexane or ethyl acetate/*n*-hexane solvent mixtures.

4. Conclusions

A new magnetically separable heterogeneous catalyst, Cu-Fe_3O_4-PAC, for CuAAC click chemistry was successfully prepared, fully characterized, and efficiently applied for the "click" regioselective synthesis of 1,4-disubstituted 1,2,3-triazoles in water at room temperature. This catalyst can easily be separated with an external magnetic field and can be reused at least five times. Its stability was proven with a hot filtration test that confirmed the stability of the catalyst. The electronic and energetic stabilities of the intermediate species that take place in the mechanistic pathway of this approach were addressed by means of QTAIM and NBO analyses.

Supplementary Materials: The supporting information can be downloaded at: https://www.mdpi.com/article/10.3390/catal12101244/s1. References [41,51–54] are listed in Supplementary Materials.

Author Contributions: Conceptualization and work strategy were designed by H.B.E.A. and S.-E.S.; synthetic work was performed by N.A. and E.M.E.M.; computational calculations were executed by H.B.E.A. and H.A.; data analysis and interpretation of the experimental and theoretical results were conducted by N.A., H.B.E.A., S.R., M.J. and S.-E.S.; writing and preparation of the original draft were carried out by N.A., H.B.E.A. and S.-E.S.; writing—review and editing were performed by N.A., M.J. and S.-E.S. All authors have read and agreed to the published version of the manuscript.

Funding: This research received no external funding.

Data Availability Statement: Not applicable.

Acknowledgments: Thanks are due to the Servicio Central de Soporte a la Investigación Experimental (SCSIE) of the Universidad de Valencia and to Centre d'Analyse et de Caracterisation (CAC) of the Université Cadi Ayyad for the instrumental facilities and support.

Conflicts of Interest: The authors declare no conflict of interest.

References

1. Huisgen, R. *1,3-Dipolar Cycloaddition Chemistry*; Wiley: New York, NY, USA, 1984; Volume 1, pp. 55–92.
2. Lazrek, H.B.; Taourirte, M.; Oulih, T.; Barascut, J.L.; Imbach, J.L.; Pannecouque, C.; Witrouw, M.; De Clercq, E. Synthesis and anti-HIV activity of new modified 1,2,3-triazole Acyclonucleosides. *Nucleosides Nucleotides Nucleic Acids* **2001**, *20*, 1949–1960. [CrossRef] [PubMed]
3. Xiong, H.; Seela, F. Stepwise "click" chemistry for the template independent construction of a broad variety of cross-linked oligonucleotides: Influence of linker length, position, and linking number on DNA duplex stability. *J. Org. Chem.* **2011**, *76*, 5584–5597. [CrossRef] [PubMed]
4. Holla, B.S.; Mahalinga, M.; Karthikeyan, M.S.; Poojary, B.; Akberali, P.M.; Kumari, N.S. Synthesis, characterization and antimicrobial activity of some substituted 1,2,3-triazoles. *Eur. J. Med. Chem.* **2005**, *40*, 1173–1178. [CrossRef] [PubMed]
5. Aly MR, E.S.; Saad, H.A.; Mohamed, M.A.M. Click reaction based synthesis, antimicrobial, and cytotoxic activities of new 1,2,3-triazoles. *Bioorg. Med. Chem. Lett.* **2015**, *25*, 2824–2830. [CrossRef]
6. Kharb, R.; Shahar Yar, M.; Sharma, C.P. New Insights into Chemistry and Anti-Infective Potential of Triazole Scaffold. *Curr. Med. Chem.* **2011**, *18*, 3265–3297. [CrossRef]
7. Duan, T.; Fan, K.; Fu, Y.; Zhong, C.; Chen, X.; Peng, T.; Qin, J. Triphenylamine-based organic dyes containing a 1,2,3-triazole bridge for dye-sensitized solar cells via a 'Click' reaction. *Dyes Pigm.* **2012**, *94*, 28–33. [CrossRef]
8. Katritzky, A.R.; Rees, C.W.; Scriven, E.F.V. *Comprehensive Heterocyclic Chemsitry II*, 2nd ed.; Pergamon Press: Oxford, UK, 1996; pp. 259–321.
9. Dorlars, A.; Schellhammer, C.-W.; Schroeder, J. Heterocycles as Structural Units in New Optical Brighteners. *Angew. Chem. Int. Ed. Eng.* **1975**, *14*, 665–679. [CrossRef]
10. Hrimla, M.; Bahsis, L.; Laamari, M.R.; Julve, M.; Stiriba, S.E. An Overview on the Performance of 1,2,3-Triazole Derivatives as Corrosion Inhibitors for Metal Surfaces. *Int. J. Mol. Sci.* **2022**, *23*, 16. [CrossRef]
11. Elazhary, I.; Boutouil, A.; Ben El Ayouchia, H.; Laamari, M.R.; El Haddad, M.; Anane, H.; Stiriba, S.-E. Anti-Corrosive Properties of (1-benzyl-1H-1,2,3-triazol-4-yl) Methanol on Mild Steel Corrosion in Hydrochloric Acid Solution: Experimental and Theoretical Evidences. *Prot. Met. Phys. Chem. Surf.* **2019**, *55*, 166–178. [CrossRef]
12. Kolb, H.C.; Finn, M.G.; Sharpless, K.B. Click chemistry: Diverse chemical function from a few good reactions. *Angew. Chem. Int. Ed.* **2001**, *40*, 2004–2021. [CrossRef]
13. Rostovtsev, V.V.; Green, L.G.; Fokin, V.V.; Sharpless, K.B. A Stepwise Huisgen Cycloaddition Process: Copper(I)-Catalyzed Regioselective "Ligation" of Azides and Terminal Alkynes. *Angew. Chem. Int. Ed.* **2002**, *41*, 2596–2599. [CrossRef]

14. Tornøe, C.W.; Christensen, C.; Meldal, M. Peptidotriazoles on solid phase: [1,2,3]-triazoles by regiospecific copper (I)-catalyzed 1,3-dipolar cycloadditions of terminal alkynes to azides. *J. Org. Chem.* **2002**, *67*, 3057–3064. [CrossRef] [PubMed]
15. Meldal, M.; Tornøe, C.W. Cu-catalyzed azide-alkyne cycloaddition. *Chem. Rev.* **2008**, *108*, 2952–3015. [CrossRef] [PubMed]
16. Bhunia, S.; Pawar, G.G.; Kumar, S.V.; Jiang, Y.; Ma, D. Selected Copper-Based Reactions for C-N, C-O, C-S, and C-C Bond Formation. *Angew. Chem. Int. Ed.* **2017**, *56*, 16136–16179. [CrossRef]
17. Aflak, N.; Ben El Ayouchia, H.; Bahsis, L.; Anane, H.; Julve, M.; Stiriba, S.E. Recent Advances in Copper-Based Solid Heterogeneous Catalysts for Azide-Alkyne Cycloaddition Reactions. *Int. J. Mol. Sci.* **2022**, *23*, 2383. [CrossRef] [PubMed]
18. Aflak, N.; Ben El Ayouchia, H.; Bahsis, L.; Anane, H.; Laamari, R.; Pascual-Alvarez, A.; Armentano, D.; Stiriba, S.-E. Facile immobilization of copper (I) acetate on silica: A recyclable and reusable heterogeneous catalyst for azide-alkyne clickable cycloaddition reactions. *Polyhedron* **2019**, *170*, 630–638. [CrossRef]
19. Wang, Z.; Zhou, X.; Gong, S.; Xie, J. MOF-Derived Cu@NC Catalyst for 1,3-Dipolar Cycloaddition Reaction. *Nanomaterials* **2022**, *12*, 1070. [CrossRef]
20. Chassaing, S.; Benneteau, V.; Pale, P. When CuAAC 'Click Chemistry' goes heterogeneous. *Catal. Sci. Technol.* **2015**, *6*, 923–957. [CrossRef]
21. Lipshutz, B.H.; Taft, B.R. Heterogeneous copper-in-charcoal-catalyzed click chemistry. *Angew. Chem. Int. Ed.* **2006**, *45*, 8235–8238. [CrossRef]
22. Vafaeezadeh, M.; Schaumlöffel, J.; Lösch, A.; De Cuyper, A.; Thiel, W.R. Dinuclear Copper Complex Immobilized on a Janus-Type Material as an Interfacial Heterogeneous Catalyst for Green Synthesis. *ACS Appl. Mater. Interfaces* **2021**, *13*, 33091–33101. [CrossRef]
23. Park, I.S.; Kwon, M.S.; Kim, Y.; Lee, J.S.; Park, J. Heterogeneous copper catalyst for the cycloaddition of azides and alkynes without additives under ambient conditions. *Org. Lett.* **2008**, *10*, 497–500. [CrossRef] [PubMed]
24. Aflak, N.; Ben El Ayouchia, H.; Bahsis, L.; El Mouchtari, E.M.; Julve, M.; Rafqah, S.; Anane, H.; Stiriba, S.-E. Sustainable Construction of Heterocyclic 1,2,3-Triazoles by Strict Click [3+2] Cycloaddition Reactions Between Azides and Alkynes on Copper/Carbon in Water. *Front. Chem.* **2019**, *7*, 81. [CrossRef] [PubMed]
25. Xiong, X.; Chen, H.; Tang, Z.; Jiang, Y. Supported CuBr on graphene oxide/Fe_3O_4: A highly efficient, magnetically separable catalyst for the multi-gram scale synthesis of 1,2,3-triazoles. *RSC Adv.* **2014**, *4*, 9830–9837. [CrossRef]
26. Lim, C.W.; Lee, I.S. Magnetically recyclable nanocatalyst systems for the organic reactions. *Nano Today* **2010**, *5*, 412–434. [CrossRef]
27. Chetia, M.; Ali, A.A.; Bhuyan, D.; Saikia, L.; Sarma, D. Magnetically recoverable chitosan-stabilised copper-iron oxide nanocomposite material as an efficient heterogeneous catalyst for azide-alkyne cycloaddition reactions. *New J. Chem.* **2015**, *39*, 5902–5907. [CrossRef]
28. Ma, Y.Z.; Zheng, D.F.; Mo, Z.Y.; Dong, R.J.; Qiu, X.Q. Magnetic lignin-based carbon nanoparticles and the adsorption for removal of methyl orange. *Colloids Surf. A Physicochem. Eng. Asp.* **2018**, *559*, 226–234. [CrossRef]
29. Wu, L.K.; Li, Y.Y.; Cao, H.Z.; Zheng, G.Q. Copper-promoted cementation of antimony in hydrochloric acid system: A green protocol. *J. Hazard. Mater.* **2015**, *299*, 520–528. [CrossRef]
30. Ai, L.; Zhang, C.; Liao, F.; Wang, Y.; Li, M.; Meng, L.; Jiang, J. Removal of methylene blue from aqueous solution with magnetite loaded multi-wall carbon nano tube: Kinetics, isotherm and mechanism analysis. *J. Hazard. Mater.* **2011**, *198*, 282–290. [CrossRef]
31. Mohan, D.; Kumar, S.; Srivastava, A. Fluoride removal from ground water using magnetic and nonmagnetic corn stover biochars. *Ecol. Eng.* **2014**, *73*, 798–808. [CrossRef]
32. Samim, M.; Kaushik, N.K.; Maitra, A. Effect of size of copper nanoparticles on its catalytic behaviour in Ullman reaction. *Bull. Mater. Sci.* **2007**, *30*, 535–540. [CrossRef]
33. Ghouma, I.; Jeguirim, M.; Sager, U.; Limousy, L.; Bennici, S.; Däuber, E.; Asbach, C.; Ligotski, R.; Schmidt, F.; Ouederni, A. The potential of activated carbon made of agro-industrial residues in NOx immissions abatement. *Energies* **2017**, *10*, 1508. [CrossRef]
34. Ahmed, M.J.K.; Ahmaruzzaman, M. A facile synthesis of Fe_3O_4-charcoal composite for the sorption of a hazardous dye from aquatic environment. *J. Environ. Manag.* **2015**, *163*, 163–173. [CrossRef] [PubMed]
35. Ahmed, M.J.K.; Ahmaruzzaman, M.; Reza, R.A. Lignocellulosic-derived modified agricultural waste: Development, characterisation and implementation in sequestering pyridine from aqueous solutions. *J. Colloid Interface Sci.* **2014**, *428*, 222–234. [CrossRef] [PubMed]
36. Thommes, M.; Kaneko, K.; Neimark, A.V.; Olivier, J.P.; Rodriguez-reinoso, F.; Rouquerol, J.; Sing, K.S.W. Physisorption of gases, with special reference to the evaluation of surface area and pore size distribution (IUPAC Technical Report). *Pure Appl. Chem.* **2015**, *87*, 9–10. [CrossRef]
37. Wu, Z.; Webley, P.A.; Zhao, D. Post-enrichment of nitrogen in soft-templated ordered mesoporous carbon materials for highly efficient phenol removal and CO_2 capture. *J. Mater. Chem.* **2012**, *22*, 11379–11389. [CrossRef]
38. Hu, X.; Jia, L.; Cheng, J.; Sun, Z. Magnetic ordered mesoporous carbon materials for adsorption of minocycline from aqueous solution: Preparation, characterization and adsorption mechanism. *J. Hazard. Mater.* **2019**, *362*, 1–8. [CrossRef]
39. Zhang, Q.; Meng, G.; Wu, J.; Li, D.; Liu, Z. Study on enhanced photocatalytic activity of magnetically recoverable Fe_3O_4@C@TiO_2 nanocomposites with core–shell nanostructure. *Opt. Mater.* **2015**, *46*, 52–58. [CrossRef]
40. de Oliveira Pereira, L.; Sales, I.M.; Zampiere, L.P.; Vieira, S.S.; do Rosário Guimarães, I.; Magalhaes, F. Preparation of magnetic photocatalysts from TiO_2, activated carbon and iron nitrate for environmental remediation. *J. Photochem. Photobiol. A Chem.* **2019**, *382*, 111907. [CrossRef]

41. López-Ruiz, H.; de la Cerda-Pedro, J.E.; Rojas-Lima, S.; Pérez-Pérez, I.; Rodríguez-Sánchez, B.V.; Santillan, R.; Coreno, O. Cuprous oxide on charcoal-catalyzed ligand-free, synthesis of 1,4-disubstituted 1,2,3-triazoles via click chemistry. *Arkivoc* **2013**, *3*, 139–164.
42. Hudson, R.; Li, C.-J.; Moores, A. Magnetic copper-iron nanoparticles as simple heterogeneous catalysts for the azide–alkyne click reaction in water. *Green Chem.* **2012**, *14*, 622–624. [CrossRef]
43. Katayama, T.; Kamata, K.; Yamaguchi, K.; Mizuno, N. A Supported Copper Hydroxide as an Efficient, Ligand-free, and Heterogeneous Precatalyst for 1,3-Dipolar Cycloadditions of Organic Azides to Terminal Alkynes. *ChemSusChem* **2009**, *2*, 59–62. [CrossRef] [PubMed]
44. Ben El Ayouchia, H.; Bahsis, L.; Anane, H.; Domingo, L.R.; Stiriba, S.-E. Understanding the mechanism and regioselectivity of the copper(I) catalyzed [2+3] cycloaddition reaction between azide and alkyne: A systematic DFT stud. *RSC Adv.* **2018**, *8*, 7670–7678. [CrossRef] [PubMed]
45. Bader, R.W.F. *Atoms in Molecules: A Quantum Theory*; Oxford University Press: Oxford, UK, 1994.
46. Tian, L.; Feiwu, C. Multiwfn: A multifunctional wave-function analyzer. *J. Comput. Chem.* **2012**, *33*, 580–592.
47. Sirohiwal, A.; Hathwar, V.R.; Dey, D.; Chopra, D. Investigation of chemical bonding in in situ cryocrystallized organometallic liquids. *ChemPhysChem* **2017**, *18*, 2859–2863. [CrossRef]
48. Peressi, M.; Fornari, M.; Gironcoli, S.D.E.; Santis, L.D.E.; Baldereschi, A. Coordination defects in amorphous silicon and hydrogenated amorphous silicon: A characterization from first-principles calculations. *Philos. Mag. B* **2000**, *80*, 515–521. [CrossRef]
49. Frisch, M.J.; Trucks, G.W.; Schlegel, H.B.; Scuseria, G.E.; Robb, M.A.; Cheeseman, J.R.; Scalmani, G.; Barone, V.; Mennucci, B.; Petersson, G.A.; et al. *Gaussian 09*; Gaussian Inc.: Wallingford, CT, USA, 2009.
50. Erdogdu, Y.; Manimaran, D.; Güllüoğlu, M.T.; Amalanathan, M.; Hubert Joe, I.; Yurdakul, S. FT-IR, FT-Raman, NMR spectra and DFT simulations of 4-(4-fluoro-phenyl)-1H-imidazole. *Opt. Spectrosc.* **2013**, *114*, 525–536. [CrossRef]
51. Wang, D.; Li, N.; Zhao, M.; Shi, W.; Ma, C.; Chen, B. Solvent-free synthesis of 1,4-disubstituted 1,2,3-triazoles using a low amount of $Cu(PPh_3)_2NO_3$ complex. *Green Chem.* **2010**, *12*, 2120–2123.
52. Siyang, H.X.; Liu, H.L.; Wu, X.Y.; Liu, P.N. Highly efficient click reaction on water catalyzed by a ruthenium complex. *RSC Adv.* **2015**, *5*, 4693–4697.
53. Sun, H.B.; Li, D.; Xie, W.; Deng, X. Catalytic Cyclization of 2,3-Dibromopropionates with Benzyl Azides to Afford 1-Benzyl-1,2,3-triazole-4-carboxylate: The Use of a Nontoxic Bismuth Catalyst. *Heterocycles* **2016**, *92*, 423–430.
54. Bragg, S.E. Cyclopentadienone Conversions to Terephthalates and Cycloadditions of Alkynes and Azides. Master's Thesis, Wright State University, Dayton, OH, USA, 2011.